Carbon Nanotubes Instruct Physiological Growth and Functionally Mature Syncytia: Nongenetic Engineering of Cardiac Myocytes

Valentina Martinelli,[†,▽] Giada Cellot,[‡,⊥,▽] Francesca Maria Toma,[§] Carlin S. Long,[∥] John H. Caldwell,[#] Lorena Zentilin,[†] Mauro Giacca,[†] Antonio Turco,[§] Maurizio Prato,[§,*] Laura Ballerini,[‡,*] and Luisa Mestroni[∥,*]

[†]International Centre for Genetic Engineering and Biotechnology, Trieste, Italy, [‡]Life Science Department and [§]Department of Chemical and Pharmaceutical Sciences, University of Trieste, Italy, [⊥]Department of Neurobiology, International School for Advanced Studies (SISSA), Trieste, Italy, and [∥]University of Colorado Cardiovascular Institute and [#]Department of Cell and Developmental Biology, University of Colorado Denver, Aurora, Colorado 80045, United States. [▽]These authors contributed equally.

ABSTRACT Myocardial tissue engineering currently represents one of the most realistic strategies for cardiac repair. We have recently discovered the ability of carbon nanotube scaffolds to promote cell division and maturation in cardiomyocytes. Here, we test the hypothesis that carbon nanotube scaffolds promote cardiomyocyte growth and maturation by altering the gene expression program, implementing the cell electrophysiological properties and improving networking and maturation of functional syncytia. In our study, we combine microscopy, biological and electrophysiological methodologies, and calcium imaging, to verify whether neonatal rat ventricular myocytes cultured on substrates of multiwall carbon nanotubes acquire a physiologically more mature phenotype compared to control (gelatin). We show that the carbon nanotube substrate stimulates the induction of a gene expression profile characteristic of terminal differentiation and physiological growth, with a 2-fold increase of α-myosin heavy chain ($P < 0.001$) and upregulation of sarcoplasmic reticulum Ca^{2+} ATPase 2a. In contrast, markers of pathological hypertrophy remain unchanged (β-myosin heavy chain, skeletal α-actin, atrial natriuretic peptide). These modifications are paralleled by an increase of connexin-43 gene expression, gap junctions and functional syncytia. Moreover, carbon nanotubes appear to exert a protective effect against the pathologic stimulus of phenylephrine. Finally, cardiomyocytes on carbon nanotubes demonstrate a more mature electrophysiological phenotype of syncytia and intracellular calcium signaling. Thus, carbon nanotubes interacting with cardiomyocytes have the ability to promote physiological growth and functional maturation. These properties are unique in the current vexing field of tissue engineering, and offer unprecedented perspectives in the development of innovative therapies for cardiac repair.

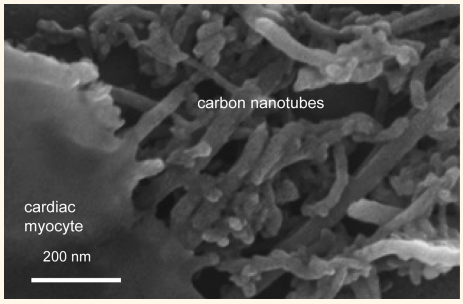

KEYWORDS: carbon nanotubes · nanoscaffolds · tissue engineering · cardiomyocytes · gene expression · cellular electrophysiology · calcium signaling

The ultimate goal of cardiac tissue engineering is the development of a bioartificial heart, an ambitious target that is unfortunately still far from being reached.[1] Nonetheless, this goal has fed a growing interest in the development of *in vitro* engineered cardiac tissues for use as model system(s). These systems are key in the investigation of cardiac development and identification of promising strategies for cardiac repair.[1] More recently, these applications have increasingly included nanotechnology-based scaffolds to promote tissue regeneration.[2,3] Of particular interest in this context is the development of scaffolds that incorporate conducting nanostructures to obtain smart biomaterials for the engineering of electrically propagating tissues.[2,4]

Our approach to address myocardial repair has been to incorporate cultures of cardiomyocytes into artificial conductive nanostructures, specifically carbon nanotubes. Recently, carbon nanotubes have attracted tremendous attention in the development of nano-bio hybrid systems able to govern cell-specific behaviors in cultured neuronal networks and explants.[5−13] Carbon nanotubes are cylindrically shaped nanostructures

* Address correspondence to prato@units.it, lballerini@units.it, luisa.mestroni@ucdenver.edu.

Received for review January 15, 2013 and accepted June 4, 2013.

Published online June 04, 2013
10.1021/nn4002193

made of one or more concentric rolled-up graphene sheets, with a diameter ranging from 1 to 100 nm. Since their discovery in 1991 by Ijima, carbon nanotubes have shown peculiar properties, such as high surface area, high mechanical strength, ultra-light weight, rich electronic properties, and excellent chemical and thermal stability.[14,15] They can be functionalized by attaching chemical compounds and used as vectors for drug delivery.[16] Once assembled into scaffolds of small fibers, they may be used as structural supports in tissue engineering.[17] The application of carbon nanotubes to biosystems has been oriented toward the use of single-walled carbon nanotubes (SWCNTs), composed of a rolled-up single graphene sheet, and multiwalled carbon nanotubes (MWCNTs), composed of numerous concentric graphene cylinders.

In our recent work, we have discovered that MWCNTs used as growth supports for neonatal rat ventricular myocytes (NRVM) increase myocyte proliferation, induce a more negative resting potential, and promote cardiomyocyte maturation.[18] Notably, fibroblast viability and proliferation were unchanged when cultured on MWCNTs.[18] These observations strengthen the conclusion by us and other investigators that carbon nanotube substrates can induce unique and diverse stimulating effects within biological systems in a cell-specific manner.[5−9,13,19] Although the mechanisms are largely unknown, the conductive properties of the carbon nanotubes indicate a potential role for electrical charges in stimulating proliferation of specific cell types.[20]

In this report, we provide evidence for the fist time for a previously unknown and unique effect of carbon nanotubes on cardiac gene expression, syncytia development, electrophysiological coupling and spontaneous calcium signaling. Based on our findings, we propose that these unique effects of carbon nanotubes on myocardial cells have remarkable potential for clinical applications in the challenging field of regenerative medicine as applied to striated muscle, from tissue engineering to innovative pacing devices for heart disease, the leading cause of morbidity and mortality in humans.

RESULTS AND DISCUSSION

MWCNT scaffolds were prepared and characterized as previously described.[7] In brief, MWCNTs of 20−30 nm (Nanostructured & Amorphous Materials, Inc.) were dispersed in *N*,*N*′-dimethylformamide (DMF) at a concentration of 0.01 mg/mL, and this solution was deposited onto the glass substrates achieving a density of the MWCNT film over the glass of about 7×10^{-5} mg/mm^2. Then, we treated the substrates for 20 min in oven under N_2 atmosphere to remove the functionalization (Supporting Information Figure 1). Even though the eventual result is the deposition of non functionalized MWCNTs on glass, this protocol has the following advantages over a direct deposition of pristine, commercial MWCNTs: (1) it allows a better dispersion of functionalized MWCNTs in a solvent and, consequently, a more homogeneous distribution on glass; (2) it allows a better adhesion of MWCNTs on the glass substrate; (3) MWCNTs are purified through the functionalization/defunctionalization procedure.[21]

Since our previous work suggested that NRVM grown on MWCNTs exhibit a more mature electrophysiological phenotype,[18] we were interested in assessing whether this might extend to the expression of genes that are established markers of physiological growth. At the same time, we also wanted to verify whether culture on MWCNTs might prevent the expression of genes associated with pathologic hypertrophy upon treatment with phenylephrine.[22−25] To this purpose, cardiomyocytes were isolated and cultured as previously described.[18] At days 1, 2, and 3 after plating, the level of expression of five key genes involved in the growth/fetal gene expression program (rat beta-myosin heavy chain (βMHC), alpha-myosin heavy chain (αMHC), A-type Natriuretic Peptide (ANP), Sarcoplasmic Reticulum Ca^{2+} ATPase 2a (SERCA2a) and Skeletal-Actin (Sk-Actin)) was quantified by transcript specific real-time PCR amplification (RT-PCR) (Figure 1A,B) both on MWCNT and gelatin scaffolds. The housekeeping gene GAPDH was used to normalize the results.

As a general observation, the gene profile of cells cultured on MWCNTs from days 1 to 3 was characterized by a progressive increase in the expression of all selected genes when compared with cells on gelatin, likely reflecting, at least in part, the overall increase in cell size (Figure 1A, Supporting Information Figure 2). This was particularly noteworthy for those genes associated with a more mature phenotype such as the αMHC gene, where NRVMs exhibited a progressive increase in expression from day 1 to day 3. As shown in Figure 1A, these changes resulted in a nearly 2-fold increase at day 3 on MWCNT compared to gelatin (P = 0.0013). This data was complemented by an increase in SERCA2a (P = 0.0059) and a lower level of ANP expression (P = 0.0065) on MWCNT compared to gelatin.[24,25] At the same time, the levels of βMHC and Sk-Actin (markers of pathologic cardiac hypertrophy) were unchanged in MWCNT compared to gelatin. When we looked at the protein expression, Western blot analysis confirmed that the levels of βMHC protein were unchanged, whereas there was an increase in SERCA2a protein in NRVM cultured on MWCNT (Figure 1C). Collectively, these results support the conclusion that MWCNT scaffolds promote a "mature gene expression profile" over time in cardiomyocytes following an initial pro-proliferative profile.[18]

Since our prior investigations suggested maintenance of the differentiated gene program favoring a more mature phenotype, we next asked whether the

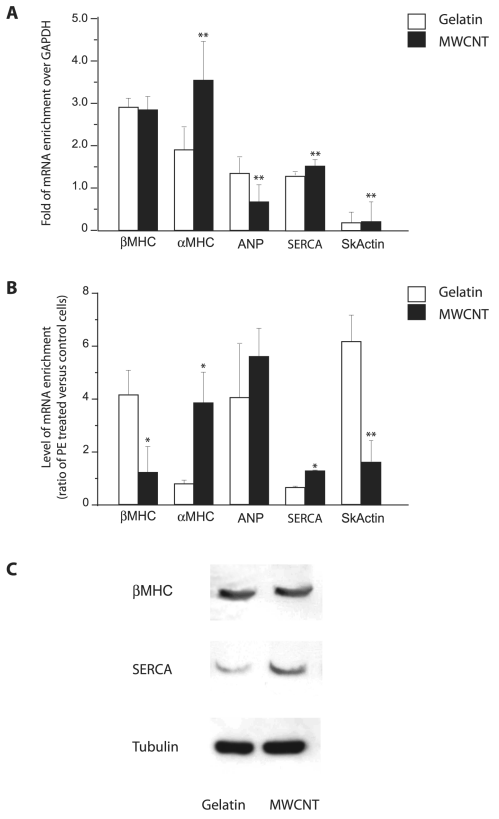

Figure 1. Physiological *vs* fetal gene expression profile of NRVM grown on MWCNTs. (A) Changes in gene expression between MWCNT and gelatin substrates in serum-growth conditions at 72 h. The histograms demonstrate up-regulation of physiological growth genes (αMHC, SERCA) *vs* pathological hypertrophy ("fetal") genes (βMHC, ANP, Sk Actin) after three days in culture of NRVMs. Bars indicate mean ± SE from 3 separate experiments. *$P < 0.05$, **<0.01. (B) Gene expression ratios for phenylephrine-treated NRVMs *vs* control NRVMs on MWCNT and gelatin substrates, respectively, at 72 h. The histogram shows that MWCNTs exert a protective effect on cardiomyocytes favoring the expression of normal (αMHC, SERCA) *vs* pathological hypertrophy genes (βMHC, ANP, Sk Actin). Bars indicate mean ± SE from 3 separate experiments. *$P < 0.05$, **<0.01. (C) Original Western blot demonstrating the increase of SERCA2a protein after 72 h on MWCNT (left) compared to gelatin (right) substrates; βMHC is equally expressed after culturing on both substrates. On the bottom, Tubulin was used as loading control.

presence of MWCNTs could alter the response to a pathologic growth stimulus. For these investigations, NRVMs were cultured for 24 to 72 h either under control serum-free conditions (Supporting Information Figure 3A) or exposed to 20 μM phenylephrine (Supporting Information Figure 3B), to induce a hypertrophic response according to previous work in our laboratory.[26,27] The first set of cells, called "Control Cells" were processed for mRNA expression, while a second set, called "Treated Cells" were exposed to phenylephrine for 24 and 48 h to induce a hypertrophic response. The histogram shown in Supporting Information Figure 3A reports the enrichment ratio of gene expression between MWCNT and gelatin conditions observed in serum-free condition in control cells. The gene expression profile was similar to what has been previously observed in normal growth condition medium for both the substrates.

In contrast, although the classic pathologic "hypertrophic" phenotype was induced in phenylephrine-treated cells grown on gelatin,[28−32] those on MWCNTs did not express this alteration in gene program. As shown in Figure 1B, at 72 h, MWCNTs (black bars) exerted an important protective role on the cardiomyocytes. In particular, αMHC gene expression was upregulated ($P = 0.034$), while βMHC and Sk-Actin were both repressed ($P = 0.027$ and $P = 0.0034$, respectively), a pattern associated with a more "adult phenotype" and typical of a mature physiological growth. Similarly, SERCA2a gene transcripts were upregulated on MWCNTs ($P = 0.0062$). Changes in ANP were not statistically significant.

Since intercellular communication is one of the important organizational features of the heart and gap junction channels form the basis of direct intercellular communication, we examined the level and localization of connexin (Cx)-43 as a marker of functionality and differentiation for cardiac myocytes grown on gelatin and MWCNT scaffolds. In human heart, Cx-43 is predominantly expressed in the ventricles and is normally located at intercalated discs.[33,34] Currently, several lines of evidence indicate that Cx-43 is not only crucial for normal ventricular function and normal impulse propagation, but its dysregulation is also implicated in various cardiac diseases with pathological left ventricular wall tension, where Cx-43 alteration may be one of the mechanisms leading to life-threatening arrhythmias.[35,36]

We investigated the organization of the cellular communication with regard to the localization of the gap-junctions through Cx-43 immunostaining 24, 48, and 72 h after plating NRVM on MWCNTs or gelatin. To distinguish between cardiac myocytes and cardiac stromal cells, we obtained cultures highly enriched in α-actinin-positive cardiomyocytes by two subsequent subplating steps (>90% purity) along with cultures of sarcomeric α-actinin-negative stromal cells (<1% α-actinin positivity). Both cultures were maintained for 1−3 days. Figure 2A shows representative images of purified neonatal cardiomyocytes stained for Cx-43 (red dots) and α-actinin−positive cells (green) at different time points in culture on MWCNTs (left panel) and gelatin (right panel) substrates. As indicated, most of the Cx-43 (red) was found associated with the plasma membrane, showing the typical gap-junction plaque structures. When syncytia with the same number of nuclei were analyzed, gap-junction Cx-43 increased with time in culture with a selective increase on MWCNT when compared to gelatin substrates. Quantitative analysis of the Cx-43-positive area indicated that the amount of Cx-43 and relative gap-junctions were significantly higher on MWCNT substrate for each of the

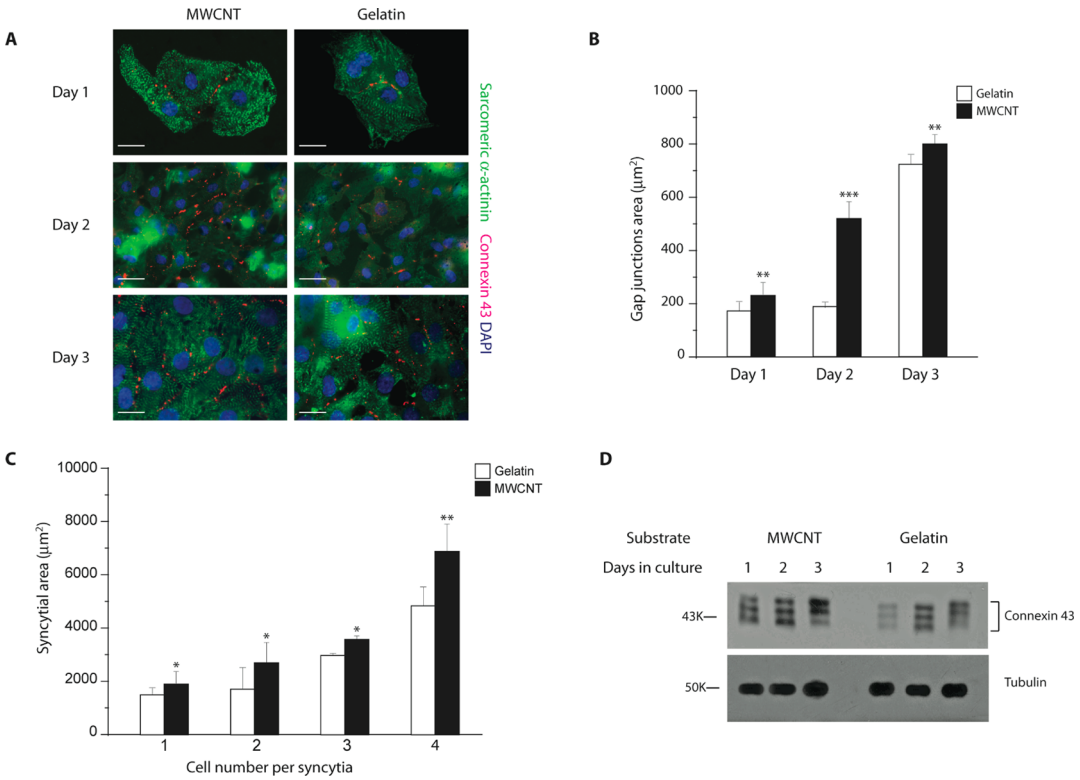

Figure 2. Gap junctions are increased in cardiomyocytes grown on MWCNT layers. (A) Cx-43 distribution on MWCNTs and gelatin scaffolds during time course experiments. Representative images of purified neonatal cardiomyocytes stained for α-Actinin (green) and Cx-43 (red) at different time points in culture. Nuclei are counterstained with DAPI (blue). The figures in each panel show fluorescence in all three channels (green/red/blue). Bars: 50 μm. (B) Quantification histogram demonstrating the increase of Cx-43 gap-junction after 24, 48, and 72 h on MWCNTs and gelatin substrates. $P = 0.052$, significance MWCNT *vs* gelatin at day 1; $P = 0.00083$, significance MWCNT *vs* gelatin at day 2; $P = 0.0034$, significance MWCNT *vs* gelatin at day 3. All data are given as mean ± SEM; results are representative of at least 6 independent experiments. (C) Quantification histogram of the total area of syncytia on MWCNT (black) and gelatin (white) substrate. All data are given as means ± SEM; results are representative of at least 6 independent experiments. Areas from the same number of cells for both growth conditions were measured between day 2 and 3. (D) Original Western blot demonstrating the increase of Cx-43 protein after 24, 48, and 72 h on MWCNT (left) and gelatin (right) substrates. At the bottom, Tubulin as a control lysate. Immunoblotting experiments using Cx-43 antibody show the presence of three major bands, which probably correspond to three differentially phosphorylated forms of the protein.[37,38].

three days of culture (Figure 2B). In particular, the amount of Cx-43 on day 2 was doubled on MWCNT ($P = 0.00083$). Next we quantified the total area of syncytia (Figure 2C): this was significantly increased (almost double in size) when NRVMs were grown on MWCNT scaffolds ($P = 0.018$). Finally, the total amount of Cx-43 protein expression was investigated by Western blot analysis at days 1, 2, and 3 on MWCNT and gelatin substrates using tubulin as control. As shown in Figure 2D, the total Cx-43 amount was consistently higher over time on MWCNT substrate compared with gelatin.

Since immunocytochemistry and Western blot experiments showed an increase in the expression of Cx43 in cardiomyocytes grown on MWCNT substrates, the functionality of gap junctions was investigated by means of dual patch clamp recordings from syncytia (experimental setting shown in Figure 3A). Dual whole cell patch clamp recordings were obtained at 37 °C in current clamp configuration, employing patch-pipettes (3.5−5 MΩ) under GΩ patch sealing. Recordings were performed after 2−3 days of *in vitro* differentiation from NRVMs that were visually identified as fused. Current clamp recordings from syncytia showed a statistically significant difference in the resting membrane potential of cells grown in the two conditions (−60 ± 2 mV, $n = 27$ for gelatin and −66 ± 2 mV, $n = 26$ for MWCNT, $P = 0.045$, Figure 3B). This more negative potential is similar to that seen earlier on a single-cell model.[18] Other passive membrane properties, such as capacitance and input resistance, were not significantly changed by growth on MWCNTs (capacitance: gelatin 398 ± 38 pF and MWCNT 429 ± 42 pF; $P = 0.59$, $n = 20$ each; input resistance gelatin 46 ± 6 MΩ and MWCNT 36 ± 6 MΩ, $P = 0.26$; $n = 20$ each). The slight increase in capacitance and decrease in input resistance are expected with the increased size of syncytia noted above.

We tested the coupling ability between pairs of NRVM cells in the syncytia as a measure of functionality of gap junctions. For these investigations, a square pulse of negative current (−0.05 nA, 100 ms) that

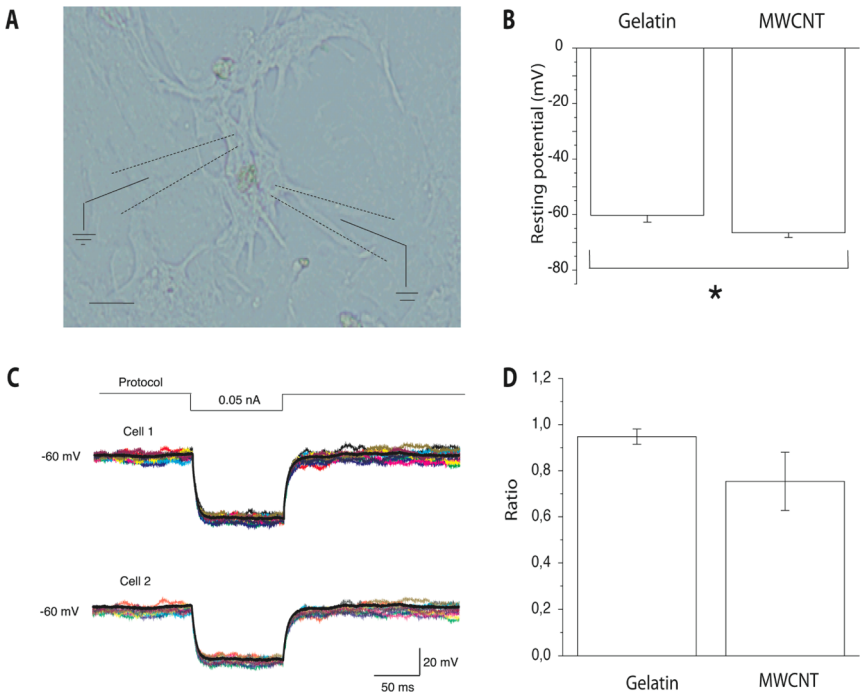

Figure 3. Gap junctions are functional in cardiomyocytes grown on MWCNT layers. (A) Bright-field image of the experimental setting for dual electrophysiological recordings from syncytia: a hyperpolarizing step is delivered by means of the first pipet (left) while the current step response is read through the second pipet simultaneously. Scale bar, 50 μm. (B) Resting potential mean value is more negative in syncytia grown on MWCNT substrates than in control ($P < 0.05$). (C) Example of dual recordings traces from a syncytium grown on MWCNT layer. Protocol (upper part), current step recorded from the pipet that delivers the hyperpolarizing stimulus (middle) and current step response detected from the second pipet (lower part). The different colors in superimposed tracings correspond to 10 trials performed in the same pair of cells. (D) Ratios between current injected in cell 2 and detected in cell 1 are reported for syncytia grown on gelatin and MWCNTs. No significant difference between substrates was seen.

induced a hyperpolarization of membrane potential in the directly stimulated myocyte was injected in the first cell (Cell 1, Figure 3C). At the same time, the amplitude of a simultaneous indirect (smaller) hyperpolarization of the membrane potential in the second cell (Cell 2, Figure 3C) was noted, indicating gap junction electrical coupling. In both growth conditions (gelatin and MWCNT), all the tested pairs of myocytes were electrically coupled. The ratio between the hyperpolarization in Cell 2 and that in Cell 1 was calculated for sample of pairs of syncytia NRVMs. On average, this ratio was similar for gelatin and MWCNT myocytes (0.95 ± 0.03 and 0.75 ± 0.13, $n = 9$ pair gelatin and $n = 9$ pair MWCNT, respectively, $P = 0.16$; Figure 3D). These results indicate the presence of functional gap junctions in both culture groups, but we did not detect differences in the percentage of coupled NRVMs, regardless of the syncytia dimensions.

Since spontaneous intracellular calcium cycling has been reported to be dependent upon cardiomyocyte maturation,[39,40] we investigated the appearance of spontaneous calcium transients in NRVM grown on MWCNT and gelatin ($n = 10$ for each). Using FURA-2 as the fluorescent Ca^{2+} indicator, we monitored the occurrence of spontaneous calcium oscillations in the presence of tetrodotoxin (10 μM), to minimize the contribution of the fast sodium current-dependent action potentials.[18] To monitor the calcium signals in single mononucleated myocytes and not in syncytia, calcium imaging experiments were performed with low density cultures (7×10^4 cell/mL).

We first measured the percentage of cells spontaneously generating calcium oscillations, then characterized the frequency and kinetics of the oscillations. In this experimental setting (lower cell density), the most cells are isolated and show asynchronous calcium activity characterized by a large variability in oscillation frequency among the detected cardiomyocyte populations. As shown in Figure 4A, we identified three categories of NRVMs on the basis of their calcium oscillating pattern: NRVM showing only sporadic, isolated events, NRVM displaying clusters of slow frequency events and NRVM capable of generating clusters of fast events.

We quantified the event frequency within each category: (1) sporadic NRVM usually display a frequency below 0.013 Hz, (2) NRVM slow frequency were in the 0.013−0.13 Hz frequency range, (3) NRVM high frequency displayed values above 0.13 Hz. On both culture substrates, we identified NRVM belonging to sporadic, low and high frequency classes. However, as shown in Figure 4B the distribution-profile is clearly changed on MWCNTs. Specifically, cells cultured on MWCNT scaffolds display a higher number of cardiomyocytes of

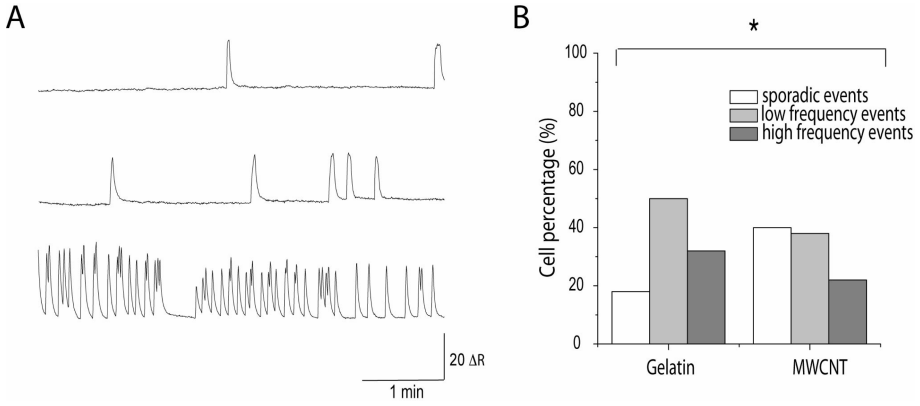

Figure 4. Calcium oscillations in cardiomyocytes grown on MWCNT and gelatin substrates. (A) Traces that exemplify the three classes of signals detected in oscillating cells: sporadic oscillating cells (upper trace), low frequency ones (middle) and high frequency ones (lower trace). (B) Distribution of the three categories for gelatin and MWCNT cells. A higher percentage of sporadic oscillating cells is present on MWCNT substrate in comparison with control ($P < 0.005$), suggesting a more mature NRVM phenotype.

the sporadic events class. This difference is statistically significant ($P = 0.009$) and suggests a decrease of spontaneous calcium oscillations, which is consistent with a more rapid maturation of the NRVM grown on MWCNT.[39] The kinetic properties of calcium events, analyzed only in the low frequency events class, were similar between gelatin and MWCNT (Table 1).

Using pharmacological tools, we tested the molecular mechanisms underlying calcium oscillations on the two substrates. In both conditions, calcium oscillations were abolished when calcium was removed from the extracellular bathing solution. Furthermore, under these calcium-free experimental conditions, addition of 10 mM caffeine (an "activator" of ryanodine receptor) induced a large intracellular calcium transient in all the tested cells. These responses were comparable between gelatin and MWCNT cultures. These results suggest an indispensable role for calcium influx in the generation of calcium oscillations in both culture groups and, at the same time, suggest the presence and maturation of functional caffeine-sensitive internal stores.

We further hypothesized that the "oscillator" is located at the cell membrane. To test this hypothesis, we applied 10 mM caffeine (5 min) to the cells in normal Tyrode solution on both substrates. After the depletion of ryanodine receptor stores induced by caffeine application, it was still possible to observe the occurrence of spontaneous transients in the internal calcium concentrations under both conditions (not shown). We also tested two likely candidate ion channels for their involvement in spontaneous calcium oscillations. Application of 40 μM nifedipine, the L-type voltage gated calcium channel blocker, failed to block the calcium oscillations in NRVMs on both substrates, inducing only a reduction in their amplitude. Similarly, treatment with 4 mM cesium alone, inhibitor of the I_{funny} channels and found to underlie the spontaneous beating of neonatal cardiomyocytes,[41] also failed to stop calcium oscillations regardless of the substrate (not shown). Therefore, calcium influx seems to be independent of both L-type calcium currents and I_{funny}.

TABLE 1. Kinetic Properties of Calcium Events in the Low Frequency Event Class

substrate[a]	gelatin ($n = 10$ cells)	MWCNT ($n = 10$ cells)
Peak Amplitude (ΔR)	17 ± 2	18 ± 2
Area (ms × ΔR)	29733 ± 5630	28384 ± 4774
Half-width (ms)	1377 ± 171	1322 ± 170
Rise Time (ms)	396 ± 52	337 ± 53
Rise Slope (ΔR/ms)	0.02 ± 0.004	0.02 ± 0.006
Decay Time (ms)	1560 ± 230	1588 ± 167
Decay Slope (ΔR/ms)	−0.007 ± 0.001	−0.007 ± 0.001

[a] ΔR is calculated as ratio of 340/380 nm excitation wavelength values (see Supporting Information).

While in our initial work we asked if cardiac myocytes will survive on a carbon nanotube scaffolds and showed that their viability and growth was indeed promoted,[18] in the current study we have explored with a series of mechanistic investigations the molecular basis of cardiac myocyte growth and maturation on MWCNT. Here, we provide evidence that carbon nanotubes induce changes in the pattern of cardiac gene expression characteristic of a more mature phenotype, highlighted by modifications in gap junction expression and function, and cell calcium signaling. Moreover, carbon nanotubes appear to exert a protective effect in response to a pathologic hypertrophy stimulus, phenylephrine. We consider our most remarkable finding to be the effect of carbon nanotubes on the expression of a group of genes critical for cardiac function and well-established markers of physiological cardiac growth. Several investigators, including our group, have previously shown both *in vitro* and *in vivo* that the heart expresses different genes and isoforms during physiological and pathological growth.[22−24] Pathological cardiac growth (hypertrophy) is characterized

by a maladaptive re-expression of the "fetal gene program", ultimately leading to deleterious alterations of the heart muscle[25,42,43] This program typically includes the downregulation of αMHC and SERCA2a genes, and upregulation of ANP and βMHC. In particular, changes in the ratio of the two myosin heavy chain isoforms, α and β, may have direct effect on the efficiency of energy production: αMHC has higher rates of ATP hydrolysis, and hearts expressing mainly αMHC have faster contractile velocities than hearts expressing mainly βMHC. This switch in expression is thought to contribute to the decreased contractile function of failing hearts.[44−47]

By studying the expression of these key cardiac genes, we provide further evidence that carbon nanotubes enhance the development and maturation of cardiomyocytes. The initial increased proliferation of NRVM cultured on MWCNT scaffolds previously reported,[18] is followed by a significant βMHC downregulation and αMHC upregulation resulting in an adult-like increase in the alpha:beta ratio (Figure 1). There is an associated upregulation of SERCA2a and Cx-43 while the expression of two other fetal program genes, Sk-actin and ANP, is diminished compared to control, providing further evidence that carbon nanotubes promote a more physiological growth phenotype.

These findings are of particular interest in the context of recent investigations on different substrates for cardiac tissue engineering. Tiburcy *et al.* recently reported that NRVM cultured with a 3D cell entrapment method of engineered heart tissues (EHTs) could provide cardiomyocytes with functional properties of native myocardium.[3] However, when gene expression was analyzed, they found no increase in the ratio of αMHC to βMHC, indicating that in their tissue-engineered conditions NRVM tended to express fetal program rather than physiological growth genes. Finally, carbon nanotube properties appear to be highly selective. In our previous studies both on neurons and cardiomyocytes, we found that the stimulation toward growth and (synapse) maturation in neurons and proliferation in cardiomyocytes affect specifically terminally differentiated cells, whereas fibroblasts and glial cells do not proliferate.[11,18]

Pathological cardiac hypertrophy can be induced *in vitro* by a variety of well-established stimuli including G-protein-coupled receptor (GPCR) agonists such as phenylephrine,[45−47] In our study, we found that carbon nanotube scaffolds interacting with cardiomyocytes protect them from the pathologic gene program induced by phenylephrine, and allow them to maintain a more physiological gene expression program. The discovery that carbon nanotube scaffold as a growth substrate can protect the heart against pathological stimuli is a novel finding and we believe it holds tremendous potential for a variety of novel therapeutic applications in heart diseases including tissue engineering and stem cells.

To better understand the effects of carbon nanotube interaction in functional domains, we explored the possibility that gap-junctions and syncytial cell properties are altered by growth on MWCNT substrate in cardiomyocyte cultures. The enhanced expression of Cx-43 and the increase in number and extension of gap junctions in syncytia further suggested a functionally more mature phenotype on carbon nanotubes compared to controls. When cultured on carbon nanotube scaffolds, we confirmed that cardiomyocytes exhibit an electrophysiological phenotype characterized by a more negative resting potential.[18] In addition, the majority of NRVM changed from low or high frequency events class to sporadic event class, in terms of spontaneous calcium transient generation. Such changes are consistent with the progression of NRVM toward more adult phenotypes,[18,39] and suggest that the environment created by MWCNTs scaffolds promote a more efficient maturation program.

The mechanistic model that explains the effects of carbon nanotubes on cardiomyocytes remains to be fully elucidated. Carbon nanotube scaffolds are unique in possessing a rough nanostructure, an extracellular matrix-like nanotopography, and electrical conductivity.[2,9,11,13] Their viscoelastic and mechanical properties, characterized by tensile strength and softness, could favor the induction of the mature gene expression program in cardiomyocytes.[48] Furthermore, carbon nanotubes have been found to modify redox signaling[49] which could activate the physiological hypertrophic response.[50] The observed changes in gene expression could be the consequence of an aging process induced by the carbon nanotube substrate in place of physiological maturation. Likewise, the changes in gene expression associated with phenylephrine treatment could instead of being protective simply document the absence of normal responses. However, taking into account our findings and our previous experience with neurons, we are tempted to speculate that the tight interaction between MWCNTs and NRVM cell membranes and the development of nanotube-cardiomyocyte hybrids may improve electrical coupling and improve growth by providing a soft artificial extracellular matrix which may ultimately facilitate cell adhesion, physiological growth and physiological maturation.[9,11,13,18]

Although there has been concern about the possible toxicity of soluble nonfunctionalized carbon nanotubes, the viability and biocompatibility of carbon nanotube scaffolds and the possibility of functionalization of carbon nanotubes to enhance their safety hold the promise for future applications of carbon nanotube-based approaches and devices in emerging strategies of drug delivery to cardiac myocytes, an approach recently shown to be feasible in neurons in a rat model of stroke.[20]

CONCLUSIONS

Cardiomyocytes which tightly interact with carbon nanotube scaffolds express a more mature molecular, cellular and electrophysiological phenotype. Based on the expression of mature *vs* fetal genes, cardiomyocyte grown on MWCNTs are protected against pathological hypertrophy. Together, these are exciting added features to the development of two- and three-dimensional nanoscale transplantable cell-enriched devices for tissue implants.[2,4,51]

METHODS

Synthesis of Multiwall Carbon Nanotubes. MWCNT of 20−30 nm (Nanostructured & Amorphous Materials, Inc.), used as received, were prepared as previously described.[7] TGA-Q500 (TA Instruments) was used to record thermo-gravimetric analysis (TGA) under N_2 or under air, by equilibrating at 100 °C, and following a ramp of 10 °C/min up to 1000 °C. In the case of defunctionalized MWCNTs, the material was analyzed after exposing to high temperature (350 °C) under N_2.

Fabrication of Glass Substrates. MWCNTs were dispersed in *N*,*N*′-dimethylformamide (DMF) at a concentration of 0.01 mg/mL, and this solution was deposited onto the glass substrates achieving a density of the MWCNT film over the glass of about 7×10^{-5} mg/mm^2. Then, we treated the substrates for 20 min in oven under N_2 atmosphere to remove the functionalization. MWCNTs thin film was characterized by sheet resistance measurements obtained using a Jandel four tips probe. The thickness of the film was measured by atomic force microscopy (AFM) and the conductivity of the material was extracted. MWCNT-coated glass substrate AFM images were analyzed by Gwyddion software (free Scanning Probe Microscope data analysis software) and average roughness calculated as rms was derived. AFM measurements were registered with a Veeco Nano Scope V in tapping mode. Phosphorus (n) doped Silicon tips with a resonance frequency of 273−325 kHz and a constant force of 20−80 N/m were used. The calculated value of conductivity for the type of MWCNT used in this study is equal to 3.82×10^5 S/cm.

Scanning Electron Microscopy. For scanning electron microscopy (SEM) measurements the samples were sputter-coated with gold in an Edwards S150A apparatus (Edwards High Vacuum, Crawley, West Sussex, U.K.), and examined with a Leica Stereoscan 430i scanning electron microscope (Leica Cambridge Ltd., Cambridge, U.K.). A SEM image of a sample of the MWCNT growth substrate used in these experiments is depicted in Supporting Information Figure 1A. A complete characterization of MWCNT-growth platforms has been previously reported.[9,11]

Culture of Neonatal Rat Ventricular Cardiomyocytes. Cardiomyocytes were isolated and cultured from six 1−3 days old pups by enzymatic digestion as previously described with minor modifications.[18,26,27,52] Protocols for tissue explants were performed in accordance with the relevant European Union legislation. Briefly, ventricles were separated from the atria using scissors and then dissociated in CBFHH (calcium and bicarbonate-free Hanks with Hepes) buffer containing 500 μg/mL of Collagenase type 2 (Worthington, Biochemical Corporation), and 1 mg/mL of Pancreatine (SIGMA).

NRVM were plated at low density in Dubecco`s modified Eagle medium (DMEM), 4.5 g of glucose supplemented with 10% horse serum, 5% bovine calf serum, 2 mg/mL vitamin B12 and cultured as previously described.[18] Cardiomyocytes were enriched (>90% purity) over nonmyocytes by two sequential preplating steps on 100-mm dishes in DME containing 10% horse serum, 5% bovine calf serum and 2 mg/mL vitamin B12 (SIGMA). Myocytes that were either in solution or lightly attached were then separated from the adherent stromal cells by gentle mechanical disaggregation and subsequently were plated at a density of 1.8×10^5 cells/mL onto 26-mm glass cover slides pretreated with MWCNT or 0.2% gelatin coated (for protein analysis, RNA, or immunofluorescence staining). The gelatin substrate was chosen as a standard and well-established control of culture conditions for neonatal rat ventricular myocytes, and to ensure in the current mechanistic experiments identical control conditions to our previous viability experiments.[18] After 12 h, the culture medium was changed and cells were subjected to the different treatments and subsequent analysis. Supporting Inforamtion Figure 1B shows a NRVM on a MWCNT scaffold.

Immunofluorescence. Cells grown on MWCNTs and on gelatin were fixed in PBS containing 3% PFA and 2% sucrose, pH 7.6 for 20 min; aldehydes were quenched with 0.1 M glycine in PBS for 5 min at room temperature. Cell were permeabilized with 1% Triton X-100 for 30 min, blocked with 2% BSA and 0.05% sodium azide in PBS (blocking buffer) for 1 h at room temperature and incubated with primary antibodies for 2 h. The primary antibodies used were as follows: rabbit polyclonal anti-connexin-43 (1:2000 SIGMA) and mouse monoclonal anti-α-actinin (sarcomeric) (EA-53) 1:100 (AbCam). Cells were then washed three times for 10 min with PBS and 0.05% Tween 20 and finally stained with secondary antibodies. Alexa Fluor 488- and Alexa Fluor 594-conjugated secondary antibodies (Invitrogen) were incubated for 45−60 min at room temperature. All washes were in PBS and 0.05% Tween 20. Samples were mounted in Vectashield plus DAPI to stain the nuclei (Vector Laboratories). For image acquisition the following objectives were used: HCX PL Fluotar 100×/1.30 NA, HCX PL apocromatic 63×/1.32−0.6 NA, HCX PL Fluotar 40×/0.75 NA, HCX PL N-Plan 20×/0.40 NA, and HCX PL N-Plan 10×/0.25 NA (all from Leica). Within each experiment, instrument settings were kept constant.

Western Blotting. For protein analysis, samples were lysed in Sample Buffer 2× and protein concentration was determined by the Bradford method (Bio-Rad Laboratories); equal amounts of protein were resolved on SDS-PAGE gels and blotted onto Immobilon-P membrane (Millipore). Immunoblots were blocked in 10% nonfat milk in PBS plus 0.05% Tween 20. Membranes were incubated with primary antibodies in PBS plus 10% of goat serum (Gibco) at 4 °C from 90 min to overnight, and washed in PBS, 0.05% Tween 20. Secondary antibodies were diluted in PBS plus 10% of goat serum and incubated with the membranes for 45 min at room temperature. Proteins were detected by enhanced chemiluminescence (GE Healthcare). The primary antibodies used were as follows: rabbit polyclonal anti-connexin-43 1:1000, (SIGMA), mouse polyclonal anti-tubulin Clone B-5-1-2, 1:10000 (SIGMA), mouse monoclonal anti-SERCA2 ATPase, 1:2000 (AbCam), mouse monoclonal anti-myosin (Skeletal, slow) Clone NOQ7.5.4D, 1:5000 (SIGMA). Secondary antibodies used were anti-rabbit and anti-mouse HRP-conjugated, 1:2000 (DAKO).

Treatment with Phenylephrine. Primary myocyte cultures were plated onto glass coverslips previously coated with MWCNT or gelatin. Myocytes were cultured in serum-free conditions for 24 h prior to all experiments in medium containing high glucose DMEM, supplemented with 10 mg/mL transferrin, 10 mg/mL insulin, 10 mg/mL BSA, 50 units/mL penicillin, 50 μg/mL streptomycin and 0.1 mM bromodeoxyuridine (BrdU), according to the Simpson laboratory protocol.[26,27] Twenty-four hours later, cells were treated for 24−48 h with 20 μM phenylephrine to induce a hypertrophic response. Control cells plated on both the substrates (MWCNT and gelatin) were treated with diluent.

RNA/DNA Isolation and Quantitative RT-PCR (qPCR). Total RNA and DNA purified from cultured neonatal rat cardiomyocytes at 1, 2, and 3 days after plating were isolated using the Trizol-method (Invitrogen) and quantified by spectrophotometry. cDNA was prepared from 1 μg total RNA by reverse transcription with MMLV-RT (Invitrogen) utilizing random hexamer primers (Invitrogen) following standard protocols (Invitrogen). RNA expression levels for beta-myosin heavy chain (βMHC), alpha-myosin heavy chain (αMHC), A-type natriuretic peptide (ANP),

sarcoplasmic reticulum Ca^{2+} ATPase 2a (SERCA2a) and skeletal-actin (Sk-Actin) were quantified with real-time TaqMan reverse transcriptase (RT)-PCR using C1000 CFX96 Real-Time System (Bio-Rad). TaqMan reactions were carried out in 96-well plates using cDNA, Taqman universal PCR master mix, predesigned and preoptimized TaqMan. Gene expression assays, including specific primers and fluorescent probes (ANP, Mm01255747_g1; βMHC, Mm00600555_m1; αMHC, RN00568304_m1; SERCA2a, Mm00437634_m1; Sk-Actin, Mm00808218_g1; glyceraldehyde-3-phosphate dehydrogenase (GAPDH, Mm99999915_g1), and water to a final volume of 50 μL, were performed according to manufacturer's instructions. GAPDH mRNA was used as an endogenous control. Each set of primer pairs was obtained from the Applied Biosystems catalogue for quantitative gene expression analysis of the specific genes of interest. RT and template controls were used to monitor for any contaminating amplification according to manufacturer (Applied Biosystems). We used the following temperature protocol: 3 min at 95 °C, 10 min at 95 °C, and 30 min at 60 °C followed by 39 cycles of 10 s at 95 °C and 30 s at 60 °C. GAPDH expression was similar in all study groups and was therefore employed to normalize for differences in RNA quantity and RT-efficiency.

Electrophysiological Recordings. Whole cell patch clamp recordings were obtained both in current and voltage clamp configurations, employing patch-pipettes (3.5−5 MΩ) under GΩ patch sealing, using a Multiclamp 700B (Axon Instruments, Foster City, CA). Recording solution contained (mM): NaCl 140, KCl 5, $MgCl_2$ 1, $CaCl_2$ 2, HEPES 10, glucose10, pH = 7.4. Patch pipettes contained (mM): 130 K-gluconate, 15 KCl, 5 NaCl, 5 Mg-ATP, 1 $MgCl_2$, 5 EGTA, 1 $CaCl_2$, and 10 HEPES, pH = 7.2. Recordings were performed from NRVM after 2−3 days of *in vitro* differentiation. Syncytia, originated from the fusion of more myocytes, were identified under visual investigation by means of their ability to contract spontaneously. Visual identification of these cells was aided by Nomarski optics coupled with an infrared microscopy system mounted on the Nikon inverted TE200 microscope.

Capacitance and input resistance were measured in voltage clamp mode at −60 mV, *via* a subthreshold 100 ms duration hyperpolarizing voltage step (5 mV). In current clamp experiments, bridge balancing was continuously monitored and adjusted. To assess the presence of gap junctions between pairs of cells, a 100 ms long lasting 0.5 nA negative current step was injected in the first myocyte and variations in membrane potential of the second cell were observed (10 trials each pair). Current and voltage clamp responses were amplified, digitized at 10−20 kHz with the pCLAMP 10 software (Axon Instruments, Foster City, CA) and stored for further analysis.

Calcium Imaging. Calcium signals were monitored in low density cultures (7×10^4 cells/mm^2) after 2 to 3 days of differentiation *in vitro*. Cells were loaded with a mixture (1:2 (v/v) in dimethylsulfoxide) of Fura-2-AM (5 μM concentration in the loading solution; Sigma-Aldrich, Italy) and 0.45% PLURONIC F127 (Sigma-Aldrich, Italy) in culture medium without serum at room temperature for 30 min. To allow the probe de-esterification, the cells were then transferred to a 37 °C incubator for additional 30−40 min. During calcium imaging experiments, cells were perfused with the saline Tyrode solution and fluorescent images were acquired at 4 Hz sampling rate. A single Fura-2-loaded coverslip was then placed in a recording chamber mounted on an inverted microscope, where it was superfused with the saline Tyrode solution at 2 mL/min. Videomicroscopy and Ca^{2+}-imaging measurements were carried out at room temperature. Cells were excited at wavelengths of 340 and 380 nm with a monochromator device equipped with integrated light source (Polychrome IV, Till Photonics). Excitation light was separated from the light emitted from the sample using a 395-nm dichroic mirror. Images of emitted fluorescence >510 nm were acquired continuously for 2400 s as a maximum (250 ms integration time for frame) by a cooled slow-scan interline transfer camera (IMAGO CCD camera; Till Photonics) and simultaneously displayed on a color monitor. The imaging system was controlled by an integrating imaging software package (TILLvisION; Till Photonics) using a personal computer. Video frames were then digitized, integrated and processed offline to convert fluorescence data into Ca^{2+} maps by computing a ratio of 340/380 nm excitation wavelength values (ΔR; integrating imaging software package, TILLvisION, Till Photonics). We recorded Ca^{2+} signals from single myocytes, not fused to form syncytia; for each experiment, four fields per coverslips were sampled and analyzed. Myocytes were visible in pseudo-colors from blue to red, corresponding to an increasing scale of Ca^{2+} concentrations.

Statistical Analysis. For immunohistochemistry quantification, data were acquired from at least 6 independent experiments by counting 100 cells per each condition. Data collected from 6 independent experiments were used to calculate mean ± standard error (SEM) and *P*-value using the Student's *t* test for unpaired samples. For real-time PCR analysis, the ΔCt was used for statistical analysis, and 2_ΔΔCt for data presentation. All electrophysiological values measured from NRVM belonging to different culture series subjected to the same experimental protocols were pooled together and expressed as mean ± SEM. For electrophysiological recordings, *n* = number of cells. Statistical analysis was carried out using the Student's and Chi Square's tests ($P < 0.05$) as appropriate.

Conflict of Interest: The authors declare the following competing financial interest(s): L.M., L.B., V.M., G.C., F.M.T., C.L., J.C., L.Z., M.P. are inventors on a filed patent regarding this work.

Acknowledgment. We are grateful to L. Masten for assistance with tissue cultures and P. D'Andrea for calcium imaging. We are grateful for the generous support of the "Foreman-Casali" Foundation, Trieste (Italy) to V.M. and L.M. Financial support from EU (NEURONANO-NMP4-CT-2006-031847 and CARBONANOBRIDGE- ERC-2008-227135, to L.B. and M.P.) and the Italian Ministry of Education MIUR (Cofin Prot. 2010N3T9M4 to MP) are gratefully acknowledged.

Supporting Information Available: Carbon nanotube scaffold and interaction with cardiomyocytes; physiological *vs* fetal gene expression profile of NRVM grown on MWCNTs; physiological *vs* fetal gene expression profile of NRVM grown on MWCNTs in serum-free conditions and after phenylephrine treatment. This material is available free of charge *via* the Internet at http://pubs.acs.org.

REFERENCES AND NOTES

1. Eschenhagen, T.; Zimmermann, W. H. Engineering Myocardial Tissue. *Circ. Res.* **2005**, *97*, 1220–1231.
2. Dvir, T.; Timko, B. P.; Kohane, D. S.; Langer, R. Nanotechnological Strategies for Engineering Complex Tissues. *Nat. Nanotechnol.* **2011**, *6*, 13–22.
3. Tiburcy, M.; Didié, M.; Boy, O.; Christalla, P.; Döker, S.; Naito, H.; Karikkineth, B. C.; El-Armouche, A.; Grimm, M.; Nose, M.; *et al.* Terminal Differentiation, Advanced Organotypic Maturation, and Modeling of Hypertrophic Growth in Engineered Heart Tissue. *Circ. Res.* **2011**, *109*, 1105–1114.
4. Dvir, T.; Timko, B. P.; Brigham, M. D.; Naik, S. R.; Karajanagi, S. S.; Levy, O.; Jin, H.; Parker, K. K.; Langer, R.; Kohane, D. S. Nanowired Three-Dimensional Cardiac Patches. *Nat. Nanotechnol.* **2011**, *6*, 720–725.
5. Mattson, M. P.; Haddon, R. C.; Rao, A. M. Molecular Functionalization of Carbon Nanotubes and Use as Substrates for Neuronal Growth. *J. Mol. Neurosci.* **2000**, *14*, 175–182.
6. Hu, H.; Ni, Y.; Montana, V.; Haddon, R. C.; Parpura, V. Chemically Functionalized Carbon Nanotubes as Substrates for Neuronal Growth. *Nano Lett.* **2004**, *4*, 507–511.
7. Lovat, V.; Pantarotto, D.; Lagostena, L.; Cacciari, B.; Grandolfo, M.; Righi, M.; Spalluto, G.; Prato, M.; Ballerini, L. Carbon Nanotube Substrates Boost Neuronal Electrical Signaling. *Nano Lett.* **2005**, *5*, 1107–1110.
8. Galvan-Garcia, P.; Keefer, E. W.; Yang, F.; Zhang, M.; Fang, S.; Zakhidov, A. A.; Baughman, R. H.; Romero, M. I. Robust Cell Migration and Neuronal Growth on Pristine Carbon Nanotube Sheets and Yarns. *J. Biomater. Sci., Polym. Ed.* **2007**, *18*, 1245–1261.
9. Cellot, G.; Cilia, E.; Cipollone, S.; Rancic, V.; Sucapane, A.; Giordani, S.; Gambazzi, L.; Markram, H.; Grandolfo, M.;

Scaini, D.; *et al.* Carbon Nanotubes Might Improve Neuronal Performance by Favouring Electrical Shortcuts. *Nat. Nanotechnol.* **2009**, *4*, 126–133.
10. Malarkey, E. B.; Parpura, V. Applications of Carbon Nanotubes in Neurobiology. *Neurodegener. Dis.* **2007**, *4*, 292–299.
11. Cellot, G.; Toma, F. M.; Varley, Z. K.; Laishram, J.; Villari, A.; Quintana, M.; Cipollone, S.; Prato, M.; Ballerini, L. Carbon Nanotube Scaffolds Tune Synaptic Strength in Cultured Neural Circuits: Novel Frontiers in Nanomaterial−Tissue Interactions. *J. Neurosci.* **2011**, *31*, 12945–12953.
12. Fabbro, A.; Cellot, G.; Prato, M.; Ballerini, L. Interfacing Neurons with Carbon Nanotubes: (Re)Engineering Neuronal Signaling. *Prog. Brain Res.* **2011**, *194*, 241–252.
13. Fabbro, A.; Villari, A.; Laishram, J.; Scaini, D.; Toma, F. M.; Turco, A.; Prato, M.; Ballerini, L. Spinal Cord Explants Use Carbon Nanotube Interfaces to Enhance Neurite Outgrowth and to Fortify Synaptic Inputs. *ACS Nano* **2012**, *6*, 2041–2055.
14. Iijima, S. Helical Microtubules of Graphitic Carbon. *Nature* **1991**, *354*, 56–58.
15. Ajayan, P. M. Nanotubes from Carbon. *Chem. Rev.* **1999**, *99*, 1787–1800.
16. Singh, R.; Pantarotto, D.; McCarthy, D.; Chaloin, O.; Hoebeke, J.; Partidos, C. D.; Briand, J. P.; Prato, M.; Bianco, A.; Kostarelos, K. Binding and Condensation of Plasmid DNA onto Functionalized Carbon Nanotubes: Toward the Construction of Nanotube-Based Gene Delivery Vectors. *J. Am. Chem. Soc.* **2005**, *127*, 4388–4396.
17. Gilmore, J. L.; Yi, X.; Quan, L.; Kabanov, A. V. Novel Nanomaterials for Clinical Neuroscience. *J. Neuroimmune Pharmacol.* **2008**, *3*, 83–94.
18. Martinelli, V.; Cellot, G.; Toma, F. M.; Long, C. S.; Caldwell, J. H.; Zentilin, L.; Giacca, M.; Turco, A.; Prato, M.; Ballerini, L.; *et al.* Carbon Nanotubes Promote Growth and Spontaneous Electrical Activity in Cultured Cardiac Myocytes. *Nano Lett.* **2012**, *2*, 1831–1838.
19. Hu, H.; Ni, Y.; Mandal, S. K.; Montana, V.; Zhao, B.; Haddon, R. C.; Parpura, V. Polyethyleneimine Functionalized Single-Walled Carbon Nanotubes as a Substrate for Neuronal Growth. *J. Phys. Chem. B* **2005**, *109*, 4285–4289.
20. Lee, H. J.; Park, J.; Yoon, O. J.; Kim, H. W.; Lee do, Y.; Kim do, H.; Lee, W. B.; Lee, N. E.; Bonventre, J. V.; Kim, S. S. Amine-Modified Single-Walled Carbon Nanotubes Protect Neurons from Injury in a Rat Stroke Model. *Nat. Nanotechnol.* **2011**, *6*, 121–125.
21. Georgakilas, V.; Voulgaris, D.; Vázquez, E.; Prato, M.; Guldi, D. M.; Kukovecz, A.; Kuzmany, H. Purification of HiPCO Carbon Nanotubes *via* Organic Functionalization. *J. Am. Chem. Soc.* **2002**, *124*, 14318–14319.
22. Lompre, A. M.; Nadal-Ginard, B.; Mahdavi, V. Expression of the Cardiac Ventricular Alpha- and Beta-Myosin Heavy Chain Genes Is Developmentally and Hormonally Regulated. *J. Biol. Chem.* **1984**, *259*, 6437–6446.
23. Kinugawa, K.; Minobe, W. A.; Wood, W. M.; Ridgway, E. C.; Baxter, J. D.; Ribeiro, R. C.; Tawadrous, M. F.; Lowes, B. A.; Long, C. S.; Bristow, M. R. Signaling Pathways Responsible for Fetal Gene Induction in the Failing Human Heart: Evidence for Altered Thyroid Hormone Receptor Gene Expression. *Circulation* **2001**, *103*, 1089–1094.
24. Jeong, M. Y.; Kinugawa, K.; Vinson, C.; Long, C. S. Afos Dissociates Cardiac Myocyte Hypertrophy and Expression of the Pathological Gene Program. *Circulation* **2005**, *111*, 1645–1651.
25. Jeong, M. Y.; Walker, J. S.; Brown, R. D.; Moore, R. L.; Vinson, C. S.; Colucci, W. S.; Long, C. S. Afos Inhibits Phenylephrine-Mediated Contractile Dysfunction by Altering Phospholamban Phosphorylation. *Am. J. Physiol.: Heart Circ. Physiol.* **2010**, *298*, H1719–1726.
26. Long, C. S.; Kariya, K.; Karns, L.; Simpson, P. C. Sympathetic Modulation of the Cardiac Myocyte Phenotype: Studies with a Cell-Culture Model of Myocardial Hypertrophy. *Basic Res. Cardiol.* **1992**, *87* (Suppl. 2), 19−31.
27. Deng, X. F.; Rokosh, D. G.; Simpson, P. C. Autonomous and Growth Factor-Induced Hypertrophy in Cultured Neonatal Mouse Cardiac Myocytes. Comparison with Rat. *Circ. Res.* **2000**, *87*, 781–788.
28. Schwartz, K.; Chassagne, C.; Boheler, K. R. The Molecular Biology of Heart Failure. *J. Am. Coll. Cardiol.* **1993**, *22*, 30A–33A.
29. Izumo, S.; Nadal-Ginard, B.; Mahdavi, V. Protooncogene Induction and Reprogramming of Cardiac Gene Expression Produced by Pressure Overload. *Proc. Natl. Acad. Sci. U.S.A.* **1988**, *85*, 339–343.
30. Nadal-Ginard, B.; Mahdavi, V. Molecular Basis of Cardiac Performance. Plasticity of the Myocardium Generated through Protein Isoform Switches. *J. Clin. Invest.* **1989**, *84*, 1693–1700.
31. Schneider, M. D.; Parker, T. G. Cardiac Growth Factors. *Prog. Growth Factor Res.* **1991**, *3*, 1–26.
32. Delcayre, C.; Swynghedauw, B. Biological Adaptation and Dysadaptation of the Heart to Chronic Arterial Hypertension: A Review. *J. Hypertens.* **1991**, *9*, S23–S28.
33. Davis, L. M.; Saffitz, J. E.; Beyer, E. C. Modulation of Connexin43 Expression: Effects on Cellular Coupling. *J. Cardiovasc. Electrophysiol.* **1995**, *6*, 103–114.
34. Beardslee, M. A.; Laing, J. G.; Beyer, E. C.; Saffitz, J. E. Rapid Turnover of Connexin43 in the Adult Rat Heart. *Circ. Res.* **1998**, *83*, 629–635.
35. Dupont, E.; Matsushita, T.; Kaba, R. A.; Vozzi, C.; Coppen, S. R.; Khan, N.; Kaprielian, R.; Yacoub, M. H.; Severs, N. J. Altered Connexin Expression in Human Congestive Heart Failure. *J. Mol. Cell. Cardiol.* **2001**, *33*, 359–371.
36. Kostin, S.; Dammer, S.; Hein, S.; Klovekorn, W. P.; Bauer, E. P.; Schaper, J. Connexin 43 Expression and Distribution in Compensated and Decompensated Cardiac Hypertrophy in Patients with Aortic Stenosis. *Cardiovasc. Res.* **2004**, *62*, 426–436.
37. Matesic, D. F.; Rupp, H. L.; Bonney, W. J.; Ruch, R. J.; Trosko, J. E. Changes in Gap-Junction Permeability, Phosphorylation, and Number Mediated by Phorbol Ester and Non-Phorbol-Ester Tumor Promoters in Rat Liver Epithelial Cells. *Mol. Carcinog.* **1994**, *10*, 226–236.
38. Musil, L. S.; Goodenough, D. A. Biochemical Analysis of Connexin43 Intracellular Transport, Phosphorylation, and Assembly into Gap Junctional Plaques. *J. Cell Biol.* **1991**, *115*, 1357–1374.
39. Gallina, C.; Dolgetta, S.; Alloatti, G.; Levi, R.; Gallo, M. P. Development of Morphology and Function of Neonatal Mouse Ventricular Myocytes Cultured on a Hyaluronan-Based Polymer Scaffold. *J. Cell. Biochem.* **2012**, *113*, 800–807.
40. Kandilci, H. B.; Tuncay, E.; Zeydanli, E. N.; Sozmen, N. N.; Turan, B. Age-Related Regulation of Excitation-Contraction Coupling in Rat Heart. *J. Physiol. Biochem.* **2011**, *67*, 317–330.
41. Er, F.; Larbig, R.; Ludwig, A.; Biel, M.; Hofmann, F.; Beuckelmann, D. J.; Hoppe, U. C. Dominant-Negative Suppression of HCN Channels Markedly Reduces the Native Pacemaker Current I(f) and Undermines Spontaneous Beating of Neonatal Cardiomyocytes. *Circulation* **2003**, *107*, 485–489.
42. Lowes, B. D.; Gilbert, E. M.; Abraham, W. T.; Minobe, W. A.; Larrabee, P.; Ferguson, D.; Wolfel, E. E.; Lindenfeld, J.; Tsvetkova, T.; Robertson, A. D.; *et al.* Myocardial Gene Expression in Dilated Cardiomyopathy Treated with Beta-Blocking Agents. *N. Engl. J. Med.* **2002**, *346*, 1357–1365.
43. Miyata, S.; Minobe, W. A.; Bristow, M. R.; Leinwand, L. A. Myosin Isoform Expression in the Failing and Non-Failing Human Heart. *Circ. Res.* **2000**, *86*, 386–390.
44. Mariner, P. D.; Luckey, S. W.; Long, C. S.; Sucharov, C. C.; Leinwand, L. A. Yin Yang 1 Represses Alpha-Myosin Heavy Chain Gene Expression in Pathologic Cardiac Hypertrophy. *Biochem. Biophys. Res. Commun.* **2005**, *326*, 79–86.
45. Yue, P.; Long, C. S.; Austin, R.; Chang, K. C.; Simpson, P. C.; Massie, B. M. Post-Infarction Heart Failure in the Rat Is Associated with Distinct Alterations in Cardiac Myocyte Molecular Phenotype. *J. Mol. Cell. Cardiol.* **1998**, *30*, 1615–1630.
46. Hefti, M. A.; Harder, B. A.; Eppenberger, H. M.; Schaub, M. C. Signaling Pathways in Cardiac Myocyte Hypertrophy. *J. Mol. Cell. Cardiol.* **1997**, *29*, 2873–2892.

47. Ng, D. C. H.; Ng, I. H. W.; Yeap, Y. Y. C.; Badrian, B.; Tsoutsman, T.; McMullen, J. R.; Semsarian, C.; Bogoyevitch, M. A. Opposing Actions of Extracellular Signal-Regulated Kinase (ERK) and Signal Transducer and Activator of Transcription 3 (Stat3) in Regulating Microtubule Stabilization During Cardiac Hypertrophy. *J. Biol. Chem.* **2011**, *286*, 1576–1587.
48. Forte, G.; P., S.; Ebara, M.; Uto, K.; Tam, J. K.; Romanazzo, S.; Escobedo-Lucea, C.; Romano, E.; Di Nardo, P.; Traversa, E.; Aoyagi, T. Substrate Stiffness Modulates Gene Expression and Phenotype in Neonatal Cardiomyocytes *in Vitro*. *Tissue Eng., Part A* **2012**, *18*, 1837–1848.
49. Sarkar, S.; Sharma, C.; Yog, R.; Periakaruppan, A.; Jejelowo, O.; Thomas, R.; Barrera, E. V.; Rice-Ficht, A. C.; Wilson, B. L.; Ramesh, G. T. Analysis of Stress Responsive Genes Induced by Single-Walled Carbon Nanotubes in BJ Foreskin Cells. *J. Nanosci. Nanotechnol.* **2007**, *7*, 584–592.
50. Santos, C. X.; Anilkumar, N.; Zhang, M.; Brewer, A. C.; Shah, A. M. Redox Signaling in Cardiac Myocytes. *Free Radical Biol. Med.* **2011**, *50*, 777–793.
51. Murtuza, B.; Nichol, J. W.; Khademhosseini, A. Micro- and Nanoscale Control of the Cardiac Stem Cell Niche for Tissue Fabrication. *Tissue Eng., Part B* **2009**, *15*, 443–454.
52. Collesi, C.; Zentilin, L.; Sinagra, G.; Giacca., M. Notch1 Signaling Stimulates Proliferation of Immature Cardiomyocytes. *J. Cell Biol.* **2008**, *183*, 117–128.